Published in final edited form as:
J Mater Chem B Mater Biol Med. 2014 December 14; 2(46): 8208–8219. doi:10.1039/C4TB01241K.

Covalent layer-by-layer assembly of hyperbranched polymers on alginate microcapsulesto impart stability and permselectivity

KM Gattás-Asfura[a], **M Valdes**[a,b], **E Celik**[c], and **CL Stabler**[a,b,d]

[a]Diabetes Research Institute, University of Miami, Miami, FL 33136 USA

[b]Department of Biomedical Engineering, University of Miami, Coral Gables, FL 33146 USA

[c]Department of Mechanical and Aerospace Engineering, University of Miami, Coral Gables, FL 33146 USA

[d]Department of Surgery and Department of Biochemistry and Molecular Biology, Miller School of Medicine, University of Miami, Miami, FL 33136 USA

Abstract

The microencapsulation of cells has shown promise as a therapeutic vehicle for the treatment of a wide variety of diseases. While alginate microcapsules provide an ideal cell encapsulation material, polycations coatings are commonly employed to enhance stability and impart permselectivity. In this study, functionalized hyperbranched alginate and dendrimer polymers were used to generate discreet nanoscale coatings onto alginate microbeads via covalent layer-by-layer assembly. The bioorthogonal Staudinger ligation scheme was used to chemoselectively crosslink azide functionalized hyperbranched alginate (alginate-hN_3) to methyl-2-diphenylphosphino-terephthalate (MDT) linked PAMAM dendrimer (PAMAM-MDT). Covalent layer-by-layer deposition of PAMAM-MDT/alginate-hN_3 coatings onto alginate microbeads resulted in highly stable coatings, even after the inner alginate gel was liquefied to form microcapsules. The permselectivity of the coated microcapsules could be manipulated via the charge density of the PAMAM, the number of layers deposited, and the length of the functional arms. The cytocompatibility of the resulting PAMAM-MDT/alginate-hN_3 coating was evaluated using a beta cell line, with no significant detrimental response observed. The biocompatibility of the coatings *in vivo* was also found comparable to uncoated alginate beads. The remarkable stability and versatile nature of these coatings provides an appealing option for bioencapsulation and the release of therapeutic agents.

Keywords

Staudinger ligation; encapsulation; diabetes; dendrimer

INTRODUCTION

The transplantation of cells to deliver therapeutic agents, such as trophic factors, hormones, antigens, and proteins, is an extensively investigated approach with broad clinical applications.[1–9] When used as a delivery agent, encapsulation of these cells within semipermeable biomaterials provides an attractive approach to protect the foreign cells from

the host immune system, where the encapsulation biomaterial permits the diffusion of the therapeutic agent into the surrounding milieu but prevents direct host cell infiltration. Of particular interest to the field is the use of encapsulated insulin secreting cells for the treatment of Type 1 Diabetes Mellitus (TIDM). Multiple studies have demonstrated the reversal of diabetes upon the transplantation of encapsulated pancreatic islets, exhibiting the promise of this approach for stabilizing blood glucose levels in the absence of anti-rejection therapy.[10–13]

Alginate is one of the most widely used biomaterials for cellular encapsulation.[14–17] Alginate is a collective term for a family of polysaccharides derived from brown algae. Alginate chains are linear binary co-polymers of β-D-mannuronic (M) and α-L-guluronic (G) acids, with a variation of sequential arrangement and composition depending on their source.[18, 19] The gelation of alginate microbeads is commonly achieved via exposure to divalent cations (typically Ca^{2+} or Ba^{2+}); however, the resulting alginate hydrogel lacks the long-term stability to withstand the mechanical and chemical strains associated with implantation, where microbead degradation and rupture commonly develops due to the slow exchange of cations with sodium ions under physiological conditions.[20, 21]

Stabilization of alginate microbeads is commonly achieved via the assembly of nano to microscale polyelectrolyte coatings on the outer alginate surface. These are assembled through layer-by-layer deposition of polymers of alternating charges, where the first layer deposited is a polycation, due to the anionic nature of alginate. Polycations typically used for alginate coatings are poly-l-lysine and poly-L-ornithine.[22, 23] Following deposition of the polycation layer, a final layer of alginate is then deposited. Although assembled in a layer-by-layer manner, it has been determined that these coatings complex to form a single polycation/polyanion shell.[16, 24, 25] As such, polycations contained within the coatings are exposed on the outer surface of the capsule. This invariably leads to the well documented decrease in biocompatibility and increased cytotoxicity of alginate capsules coated with these polycations.[26–30]

In this study, we sought to explore the potential of covalent layer-by-layer assembly of complementary polymers for stabilization of alginate capsules. Covalent layer-by-layer assembly provides a mean to enhance the stability of coatings via interpolymer covalent bonding, as well as intimate nanoscale control over layer thickness.[31–34] Further, this approach provides flexibility in polymer selection, where moderately charged or even neutral polymers can be employed. Herein, we explored the use of highly branched polymers to assemble an architecture expressing bioorthogonal functionality and tailored physiochemical properties for generating nanoscale coatings onto hydrogels. Layer-by-layer assembly of hyperbranched and/or dendrimer polymers, first explored by Decher and co-workers[35, 36], are highly desirable for biomedical applications, as their facile nature provides substantial variation in function and structure, while their high density of terminal groups provides increased availability for interaction with alternating layers.[37] In our laboratory, we have developed hyperbranched alginate and poly(amido amine) (PAMAM) dendrimers functionalized with the complementary Staudinger ligation reactive groups, azide and methyl-2-diphenylphosphino-terephthalate (MDT), respectively (Figure 1A). The bioorthogonal Staudinger ligation scheme for covalent bond formation is particularly

appealing for biological studies, as the reaction can proceed in an aqueous environment, under defined environmental conditions (e.g. temperature 25–37 °C, pH 7–7.5, osmolarity ~300 mOsM), and involve non-native chemical handles and nontoxic catalysts and/or reaction by-products.[38, 39] We have demonstrated the capacity of these hyperbranched polymers to form stable, discreet, and nanoscale coatings via covalent layer-by-layer assembly, both on idealized surface and cell clusters[40]. Herein, we applied these coatings to alginate microbeads, to evaluate their potential for providing a stable, permselective, and biocompatible coating. Physiochemical properties of the resulting coating were evaluated via permeability, swelling, and cytotoxicity studies. Further, biocompatibility of the coatings was evaluated in a rodent model. The potential of these nanoscale, covalent, layer-by-layer assembled coatings to provide a useful platform for bioencapsulation is discussed.

EXPERIMENTAL

Materials Sourcing, Polymer Fabrication, and Solutions

For formation of alginate based hydrogels, alginate or alginate functionalized with azide (but not hyperbranched), sourced from UP MVG (Pronova, NovaMatrix, NJ), was used. The content and distribution of M and G units were determined by ^{1}H NMR spectroscopy and provided by the manufacturer. For UP MVG, the fraction of G units (F_G) was 0.6889. The fraction of diads F_{GG}, $F_{MG/GM}$, and F_{MM} were 0.58, 0.11, and 0.20, respectively. The fraction of triads F_{GGG}, $F_{MGG/GGM}$, F_{MGM} were 0.54, 0.039, and 0.070, respectively, with a $N_{G>1}$ of 15.82. Synthesis of alginate-N_3 (not hyperbranched) used to fabricate microbeads was prepared as previously described.[41, 42] In brief, 50 mg of UP MVG sodium alginate, 14 mg NHS and 62 mg MES were dissolved in 5 mL de-ionized water. A 200 μL solution of 376 mM N_3-PEG-NH_2 (M_w 372 g/mol) was added, followed by 116 mg EDC (116 mg in 200 μL water, 0.60 mmol, prepared fresh), 25 min stirring, and added slowly (within 20 min) 270 μL of 1 M NaOH. Purification was achieved via 4 days dialysis (10,000 MWCO membrane) against 600 mL water, which was changed three times a day. During the first 3 days, NaOH (5 μL of 5 M) and NaCl (250 μL of 4 M) were added twice daily to the alginate-containing solution. Larger batch sizes (10×) were also fabricated using this method. The remaining solution was filtered through a 0.2 μm membrane (Pall Corp) and freeze-dried. Purity and functionalization has been reported previously[9], where purity was a minimum of 97%, with an average azide modification of 11 % (percent modification of alginate caboxylate groups) or 149 N_3 per alginate mol ratio.

For formation of covalent layer-by-layer coatings onto the alginate hydrogel microbead, hyperbranched alginate-azide (termed “alginate-hN_3” in this study) and functionalized PAMAMs (labeled according to the degree of functionalization of terminal groups with MDT/glutaric anhydride, see Table 1) were prepared as previously described[40]. For alginate-hN_3, UP VLVG sodium alginate (PRONOVA, NovaMatrix) was used. For UP VLVG, the fraction of G units (F_G) was 0.6661. The fraction of diads F_{GG}, $F_{MG/GM}$, and F_{MM} were 0.56, 0.11, and 0.22, respectively. The fraction of triads F_{GGG}, $F_{MGG/GGM}$, F_{MGM} were 0.51, 0.043, and 0.067, respectively, with a $N_{G>1}$ of 13.88. Briefly, 800 mg of 1-ethyl-3-[3-(dimethylamino)propyl]-carbodiimide hydrochloride (EDC) followed by 200 mg of 3,5-dicarboxyphenylglycineamide (in 3.8 mL of 0.42 M NaOH, 267 μL/min) were

added to 200 mg UP VLVG alginate, 16 mg of N-hydroxysuccinimide (NHS), and 240 mg of 2-(N-morpholino)ethanesulfonic acid (MES) dissolved in 20 mL of water. After 25 min, 240 μL of 5 M NaOH was added at 2.67 μL/min. Hyperbranched alginate was precipitated with 40 mL acetone, dissolved in 4 mL of 50 mM NaCl, precipitated with 8 mL acetone, and dried under reduced pressure. Next, 50 mg of hyperbranched alginate and 50 mg of H_2N-PEG-N_3 (M_w 372 g/mol) were reacted with 125 mg EDC in 5 mL purified water containing 5 mg NHS, 30 mg MES, and either 0 or 2 mg of fluorescein-5-thiosemicarbazide. After 20 min, 30 μL of 5 M NaOH was added at 1 μL/min. Hyperbranched alginate-azide was precipitated with 20 mL acetone, dissolved/precipitated twice in 3 mL of 50 mM NaCl/15 mL acetone, dried under reduced pressure, purified by dialysis (10 kDa MWCO, against 500 mL water replaced every 20 min for 2 h, 10 μL NaOH and 200 μL 1 M NaCl were added to the alginate solution during the first hour every 20 min), filter-sterilized, and freeze-dried.

For the functionalization of poly(amidoamine) (PAMAM) dendrimers, generation 5 PAMAM (1 mL of 5 % in CH_3OH, 39.85 mg) was reacted with 14 mg of 4-pentafluorophenyl ester of 1-methyl-2-(diphenylphosphino)terephthalic acid in 0.5 mL anhydrous dichloromethane (DCM, injected drop-wise) for 30 min under argon atmosphere (PAMAM 15/0). For PAMAM 15/20 or 15/40, 25 μL of triethylamine in 0.5 mL DCM was injected followed by 4 or 8 mg (respectively) of glutaric anhydride in 0.5 mL DCM (injected drop-wise). After 30 min, 20 μL glacial acetic acid was added, the product precipitated with 10 mL diethyl ether, dissolved/suspended in 1 mL of 50 % v/v DCM in methanol, precipitated with 10 mL diethyl ether, dried under reduced pressure, dissolved in 2 mL water with 20 μL glacial acetic acid, purified by dialysis (10 kDa MWCO, against 500 mL water replaced every 20 min for 2 h). 100 μL of 1 M NaCl was added to the alginate solution every 20 min for the first hour, filter-sterilized, and freeze-dried. ATR-FT-IR spectra characterized MDT group (1719, 746, and 697 cm^{-1}) and amide bonding (1637 and 1539 cm^{-1}), while the degree of functionalization was determined via NMR peak integration ratio between aromatic (6.5–8.2 ppm) or GA (1.83 ppm) against PAMAM (2.07–3.66 ppm) protons. Characterization data of selected MDT and GA functionalized PAMAM dendrimers are summarized in Table 1. Of note, the surface net charge listed for the specific dendrimer assumes every primary amino or carboxylate group is charged, thus the true net charge depends on pH of the solution

Fabrication of alginate or alginate-azide microbeads without and with beta cells

Standard alginate or alginate-N_3 microbeads were fabricated using a modification of the protocol originally developed by Sun.[43] To prepare the alginate solutions, 1.0 % w/v alginate or alginate-N_3 was dissolved in phosphate-buffered solution (PBS, Mediatech), the pH of the solution was adjusted to 11 with 5 M NaOH, stirred until clear, and slowly recovered to pH 7.4 via equimolar amount of HCl. A parallel air flow bead generator (Biorep, Inc. Miami, FL) was used to fabricate the microbeads in Ba^{2+} containing MOPS buffer. The size of the droplets was controlled by a parallel airflow generator (10 kPa pressure of air; 1 inch distance from the needle to gelation solution) and manual force applied to the syringe. The beads were exposed to the gelation solution for 10 min to form a stable hydrogel. The barium solution was aspirated and the beads were then rinsed with PBS four times to remove excess barium. For coating and permselectivity studies, resulting

microbead diameters averaged 757 ± 35 μm (n = 19). Microbeads were stored in PBS prior to bead swelling and/or chelation assays.

For microbeads containing cells, MIN6 cells were used. MIN6 cells (subclone C3, courtesy of Dr. Valerie Lilla and Alejandra Tomas)[44] were cultured as monolayers in T-flasks and fed every 2–3 days with fresh medium comprised of Dulbecco's modified Eagle's medium (DMEM) supplemented with 10 % fetal bovine serum (FBS; Sigma), 1 % penicillin-streptomycin (P/S), 1 % L-glutamine and 0.001 % (v/v) β-mercaptoethanol. MIN6 cells were harvested from monolayer cultures using trypsin-EDTA (Sigma, St. Louis, MO) and suspended in either polymer solution at a density of 2.5×10^6 cells/ml of 1 % w/v alginate polymer solution. Viable cell counts for measurement of loading cell density were performed via trypan blue (Sigma, St. Louis, MO) exclusion method. Following the homogeneous distribution of the cells within either alginate solution, the cell/polymer suspension was immediately extruded through the air flow bead generator to form microbeads, as described above. Following an 8 min exposure to the barium gelation solution and PBS rinse (4 times), the cell-containing microbeads were washed in culture media described above. Beads were subsequently coated in PAMAM/alginate microbeads prior to culture in non-cell culture treated plates in a humidified 37 °C, 5 % CO_2/95 % air incubator for 48 h prior to assessment. Resulting microbead diameters for averaged 815 ± 34 μm (n = 24).

Coating of alginate or alginate-azide microbeads with PAMAM/alginate or PLL/alginate

For layer-by-layer assembly of PAMAM and alginate-hN_3 onto the alginate microbeads, microbeads were first incubated in the PAMAM polymer solution (3 mg/mL in PBS buffer) for 10 min at 37 °C, following by rinsing (3×) with PBS. Subsequently, a layer of alginate-hN_3 was added via incubation of PAMAM coated bead with alginate-hN_3 polymer solution (3 mg/mL in PBS buffer) for 10 min at 37 °C, following by rinsing (3×) with PBS. This process was repeated until the desired number of layers was achieved. A plastic disposable Pasteur pipet was frequently utilized to stir and separate the microbeads to prevent aggregation. The polymer solution was supplemented with glucose (3 mg/dL) when coating microbeads containing MIN6 cells.

Microbeads coated with poly-L-lysine and standard alginate (PLL/Alg) served as the control group. To generate the PLL coating, microbeads were incubated in 0.05% (wt/v) of poly-L-lysine (MW 30,000–70,000, Sigma Cat #P2636) in PBS buffer for 6 min at room temperature. Excess PLL was rinsed away with multiple washes with PBS buffer. Microbeads were subsequently incubated in 0.15% of standard alginate (UP MVG) for 4 min at room temperature, followed by extensive rinsing in PBS.

Cell-free coated microbeads were stored at 37 °C in PBS. For cell loaded, microbeads were cultured as described above. For formation of microcapsules, coated microbeads were treated with 50 mM EDTA solution in MOPS buffer (1×, pH 7.4) for 15 min in order to chelate barium ions from the alginate core. The resulting capsules were rinsed three times with PBS (1×, pH 7.4) for 5 min. Following rinsing, microbeads were assessed for swelling.

Swelling and Permeability of Capsules

For swelling testing, the diameter of multiple (at least 4) coated beads in PBS was measured before and 1 h after EDTA treatment utilizing the SZX7 stereo microscope (Olympus). Degree of swelling was calculated from the ratio of capsule diameter over bead diameter.

Permeability testing was conducted on coatings following EDTA treatment, to minimize the contribution of the alginate hydrogel on permselectivity. For permeability testing, coated alginate or alginate-N_3 microcapsules (following EDTA treatment) were placed on glass bottom petri dishes and incubated for 2 h in 0.1 mg/mL of FITC-dextran of different molecular weights (4, 10, 40, 70, 150, 250, 500, or 2000 × 10^3 g/mol) in PBS buffer. Ethidium bromide (0.2 μL of Invitrogen red dead stain for cells) was utilized to fluorescently label the capsules. After 2 hr, microcapsules were subsequently imaged via fluorescence confocal microscopy. Confocal images were cross-sections at 100 μm depth from bottom of the microcapsules. The degree of FITC-dextran permeability through the different capsules was quantified by dividing the green luminosity inside the beads over that on the outside utilizing the histogram tool of Adobe Photoshop, hence accounting for variations in fluorescent label concentration with the change in dextran molecular weight. Values are expressed as the average of measurements from at least three different beads per experimental condition. Measurements were collected again after 24 h of incubation to verify that equilibrium was achieved within that 2 h incubation. Variation between 2 and 24 h measurements were less than 8%.

The permselectivity or molecular weight cut-off of the capsules was experimentally identified when the % permeability for a particular dextran molecular weight was < 10%. The corresponding hydrodynamic radius of the dextran was theoretically determined using the following published formula[45]:

$$R_h = 0.026(MW)^{0.495} \quad [1]$$

where R_h is the hydrodynamic radius of the dextran in nm and MW is the molecular weight in g/mol.

Atomic Force Microscopy

A commercial atomic force microscope (MFP-3D-BIO, Asylum Research) was used to obtain high-magnification images of the polymer coatings. In order to hold the sample steady during AFM imaging, the microbeads were trapped on glass slides by agarose films. Briefly, a coated microbead was placed on a glass slide and a warm solution of 1.5% agarose in water was applied around the microbead using a stereomicroscope. The microbead was held stable in place upon agarose gelation by cooling. Care was taken not to contaminate the microbead surface during this process. The agarose height was ~75 – 80% of the bead's height, which corresponds to an exposure area for AFM imaging of ~ 640 μm (see Supplementary Materials for images of beads embedded in agarose). The AFM tip was positioned above the trapped microbead immersed in PBS and scanned in the contact mode to acquire surface topography. A pyramidal, silicon nitride AFM cantilever tip (nominal spring constant 0.01 N/m, MLCT series, Bruker AFM Probes) was used to image all

samples. All images were acquired with a scan size of 10 μm and a resolution of 256 × 256 points. RMS roughness (*Rq*) of the surfaces was measured on the AFM height images at 5 different locations using the equation; $R_q = \sqrt{\frac{\sum (Z_i - Z_{ave})^2}{N}}$ where z_{ave} is the average of the elevation (*z* value) within the given area, z_i is the elevation for a given point, and *N* is the number of data points within the given area.

Cytocompatibility and insulin release of encapsulated beta cells

A two-color fluorescent viability and cytotoxicity kit (Molecular Probes) was used to evaluate cell viability. Viable (active intracellular esterase) cells stain fluorescent green with calcein-AM and dead (lost plasma membrane integrity) cells stain fluorescent red with ethidium homodimer-1 dye. Encapsulated cells and dyes were co-incubated in DMEM media for 1 h followed by imaging with confocal microscope. Of note, interactions between the PAMAM/alginate coating and the ethidium homodimer-1 dye have been documented. Hoechst dye was added to label cell nuclei in an effort to delineate coating staining from dead cell staining.

Glucose stimulated insulin release (GSIR) consisted of aliquoting 130 microbeads per group (127 ± 37 microbeads/group) in 1 mL Krebs buffer with low glucose (60 mg/dL) for 30 min in a 12-well plate and incubator. The same microbeads were then incubated in Krebs buffer with high glucose for 3 h. The high glucose (300 mg/dL) Krebs buffer was collected and the amount of insulin was determined utilizing the mouse insulin Elisa quantification kit.

Biocompatibility assay

All animal studies were reviewed and approved by the University of Miami Institutional Animal Care and Use Committee. All procedures were conducted according to the guidelines of the Committee on Care and Use of Laboratory Animals, Institute of Laboratory Animal Resources (National Research Council, Washington DC). Animals were housed within microisolated cages in Virus Antibody Free rooms with free access to autoclaved food and water at the Department of Veterinary Resources of the University of Miami. Male C57BL/6J mice, between 7–9 wks of age (Jackson Laboratory), were used as recipients. This strain has a demonstrated robust host response to materials and is a common choice used for biocompatibility studies, particularly those involving alginate capsules[46–48]. Groups consisted of uncoated microbeads, 6-layer coating, and 7-layer coating using alternate PAMAM 15/0 and hyperbranched alginate-azide layers. Under general anesthesia (isoflurane USP, Deerfield, IL), a lower mid-line incision was made and microbeads (1–1.5 mL) were introduced into the peritoneal cavity. The incision was then stapled closed. Microbeads were retrieved after 21 days post implantation via lavage, rinsed with PBS, fixed, sectioned, and stained with hematoxylin and eosin for microscopic imaging.

Statistics

All data analysis used Excel (Microsoft, USA), with statistical analysis and graphing via GraphPad Prism (GraphPad Software, Inc., USA). Data are presented as mean ± SEM.

Results were analyzed via one or two-way ANOVA, with Bonferroni or Tukey post-host analysis. Observations were considered to be statistically significant with $p < 0.05$.

RESULTS AND DISCUSSION

Formation of coatings onto alginate microbeads

Initial studies sought to explore the capacity to coat hydrogel microbeads, in a layer-by-layer manner, using complementary functionalized polymers that are covalently linked via Staudinger ligation (Figure 1A). The formation of covalent layer-by-layer coatings onto the alginate microbeads was explored using two alginate hydrogel platforms: standard alginate or alginate-N_3. The alginate-N_3 employed for microbead generation was not hyperbranched; a portion of carboxylate groups of alginate were simply functionalized with linear H_2N-PEG-N_3. Both microbeads were generated via ionic gelation. Resulting microbeads were coated with layers of PAMAM and alginate, functionalized with methyl-2-diphenylphosphino-terephthalate (MDT) and azide, respectively, via step-wise incubation (Figure 1B). For all coatings, PAMAM was used as the base layer (Figure 1). In this study, PAMAM dendrimer (generation 5) was used, whereby 15 % of primary amino end groups on PAMAM was functionalized with MDT[40]. To explore the contribution of net charge on layer formation, a subset of the remaining primary amino groups on the PAMAM-MDT was subsequently modified with glutaric anhydride (GA). GA functionalization was varied from 0 to 20 to 40%, designated as PAMAM 15/0, PAMAM 15/20, and PAMAM 15/40, respectively, resulting in a net dendrimer surface charge of +110 to +51 to −3, as previously published (see Table 1 for summary)[40]. For interim layers, hyperbranched alginate azide, termed alginate-hN_3, was employed (Figure 1B). As previously described, a carbodiimide-based coupling protocol was utilized to hypergraft branched polymeric chains of 3,5-dicarboxyphenylglycineamide onto the alginate backbone, which were subsequently functionalized with azide via treatment with a linear, heterobifunctional poly(ethylene glycol), expressing a primary amino and an azido end group[40]. The molecular weight of the PEG-N_3 linker, and hence the length of the hyperbranched azide functionalized arm, could be modified to explore its impact on the resulting coating. Molecular weights of 300 and 600 g/mol were investigated in this study. The use of hyperbranched and dendrimer polymers, with increased presentation of reactive groups, was found to enhance the efficiency and competency of covalent layer-by-layer formation on idealized planar surfaces[40].

Resulting coatings were visualized with confocal microscopy via FITC labeling of the hyperbranched alginate azide. As illustrated in Figure 1C, nanoscale coatings were generated on alginate microbeads, with coating uniformity and intensity increasing with subsequent layers. Increased net positive charge of the PAMAM correlated with increased uniformity at 2 and 4 layers; however, by 6 layers, coatings generated by any of the PAMAM forms were comparable, with uniform and complete coatings observed. Surprisingly, the presence of azide groups on the base alginate microbead did not significantly impact PAMAM deposition. Resulting coatings were highly stable, even after several weeks of storage at room temperature.

Stability of coatings following liquification of inner alginate core

Of interest to the generation of a versatile coating platform is the impact of the coatings on bead stability. To explore the contribution of the coatings to enhance alginate stability, alginate or alginate-N_3 microbeads were chelated via EDTA following layer-by-layer coating to remove barium ions and liquefy the inner alginate hydrogel, resulting in alginate microcapsules. The stability of microcapsules was assessed via percent swelling following chelation. For comparison, standard alginate/poly-l-lysine (PLL) coated microbeads were also evaluated. If coatings were not complete or stable, liquification of the inner alginate core would result in ruptured or dissolved beads. Following chelation, a significant increase in the magnitude of swelling was observed, when comparing alginate microcapsules to alginate-N_3 microcapsules, regardless of the coating type (see Table 2). The degree of swelling for alginate-N_3 capsules ranged from −2 to 32%, while standard alginate capsules ranged from 30 – 44%. This observed increase in swelling for standard alginate capsules is similar to that reported in studies evaluating PLL coatings.[49] Coated alginate-N_3 microcapsules were reasonably stable following chelation, with minimal breakage observed with handling; however, coated alginate microcapsules were fragile and susceptible to breakage, similar to published reports for standard PLL coatings.[50, 51] This increased fragility of the standard alginate microcapsules is likely attributed to the high degree of swelling following chelation, resulting in mechanically stressed coatings. The significant decrease in swelling for alginate-N_3 versus alginate microbeads is postulated to be due to changes in the alginate chain properties due to the functionalization of the carboxyl groups with PEG-N_3. The 11% functionalization of the alginate to form alginate-N_3 has been found to result in less compact beads following gelation, likely due to the interference of the PEG-N_3 in the formation of the classic “egg-box” interactions between alginate chains and the gelation cations to form rod-like cross-linked complex.[41] Hence, the less dense gelation network of the alginate-N_3 microbead experiences less swelling following chelation and subsequent liquification, than standard alginate microbeads. Further, the functionalization of the carboxyl groups with PEG-N_3 decreases the net anionic charge of the alginate. While the exact decrease in net anionic charge cannot be measured, given this is highly dependent on the exact monomer groups of the alginate and the pH, it can be concluded that 11% functionalization of the carboxylate groups with neutral PEG-N_3 would result in a subsequent reduction in charge, which would lead to decreased electrostatic repulsion for alginate-N_3 chains, when compared to standard alginate. Overall, the decreased gel compactness and electrostatic repulsion of alginate-N_3 chains likely contributes to the decreased overall swelling of these microcapsules following liquification of the inner alginate core.

Evaluation of the contribution of the layer-by-layer coating on the degree of swelling found significant variation within most groups (Table 2). For coatings on alginate-N_3 microcapsules, control PLL/Alg coated beads exhibited no swelling, while swelling for PAMAM/alginate-hN_3 coatings formed using PAMAM 15/20 and 15/40 were equivalent and were significantly lower than those formed using PAMAM 15/0. For coatings onto standard alginate microcapsules, PAMAM/alginate-hN_3 coatings formed using PAMAM 15/20 exhibited the lowest overall swelling, followed by those formed using PAMAM 15/40

and then PAMAM 15/0. Coatings formed using PLL/Alg were statistically equivalent to PAMAM 15/40 coatings.

Increasing the layer number from 6 to 12 total layers resulted in enhanced stability of the microbeads, as a significant decrease in swelling was observed for all groups. Increasing the length of the azido-functionalized PEG linker (300 to 600 g/mol) on alginate-hN_3 resulted in a 2-fold increase in % swelling; demonstrating than varying the layer spacing of the PAMAM/alginate-hN_3 coatings impacts their capacity to remodel under osmotic stress. Overall, these studies demonstrate the stability of covalent layer-by-layer coatings formed using alternating PAMAM/alginate-hN_3 layers, even following substantial swelling of the base coating material. Further, the stability of the coating can be modulated by layer number and spacing.

Permselectivity of resulting coatings on microcapsules

Modulation of the permselectivity is a critical parameter in the application of biomaterials for drug delivery or cellular encapsulation. To evaluate the capacity of the layer-by-layer coating to impart permselectivity, the inner hydrogel core of the coated microbeads was chelated. This provides a means to delineate the contribution of the base alginate hydrogel on permselectivity. Coated microcapsules were then incubated within FITC-dextran solutions of variable molecular weights (i.e. 4×10^3 – $2{,}000 \times 10^3$ g/mol). PAMAM within the coating was labeled via addition of ethidium homodimer-1 to permit clear identification of the capsule periphery (Figure 2A–D).[40] Image analysis characterized the degree of infiltration of FITC-dextran, compared to background, to quantify the % permeability. Size exclusion was established when the measured % permeability was less than 10%. As summarized in Figures 2E–F, coated capsules exhibited variations in degree of permselectivity, according to the PAMAM derivative used for the coating and the microcapsule base employed (i.e. alginate-N_3 (Figure 2E) or alginate (Figure 2E)). Coatings using PAMAM 15/0 and PAMAM 15/20 exhibited the highest permselectivity, where dextrans of MW $\geq 40{\times}10^3$ were excluded, regardless of the base microcapsule material. PAMAM 15/40 coatings on alginate-N_3 capsules demonstrated increased permeability to larger dextrans, with MW as high as 250×10^3 g/mol, permitted within the capsule, while PAMAM 15/40 coatings on standard alginate capsules were more restrictive ($< 70 \times 10^3$ g/mol).

Table 3 summarizes the overall permselectivity of the coatings, correlating this to size range exclusion using the theoretical relationship between dextran molecular weight and its hydrodynamic radius.[45] In general, PAMAM/alginate-hN_3 coatings fabricated using PAMAM 15/0 or 15/20 were more permselective than coatings formed using PAMAM 15/40, regardless of the base capsule material. In comparison to PLL/alginate coated microcapsules, covalent layer-by-layer coatings formed using PAMAM/alginate-hN_3 were generally more permselective, with PLL/Alg coatings on standard alginate restricting dextrans of MW $> 70{\times}10^3$ g/mol and PLL/Alg coatings on alginate-N_3 restricting dextrans of MW $> 2{,}000{\times}10^3$ g/mol (full permeability results for standard PLL/alginate coatings are summarized in Supplementary Materials).

To further investigate the adaptable nature of these covalently linked coatings, we explored the contribution of: 1) the number of total layers (Figure 3A); 2) the length of the PEG linker used to link azide onto the hyperbranched alginate (Figure 3B); and 3) the base alginate microcapsule material (Figure 3C) on coating permselectivity. For these studies, covalent layer-by-layer coatings were formed using PAMAM 15/40. As expected, an increase in the number of layers from 6 to 12 resulted in a more restrictive capsule (Figure 3A), with a significant decrease in migration of the dextran into the capsule between $10 \times 10^3 \leq MW \leq 250 \times 10^3$, although the exclusion cutoff remained the same at $500{\times}10^3$ g/mol (R_h = 17.2 nm). Increasing the length of the PEG-N_3 linker on the alginate-hN_3 (Figure 3B) also resulted in modulation of permselectivity, whereby increased migration of dextran was observed when $MW \leq 250 \times 10^3$. This increased permselectivity is likely due to the increased thickness of the coatings, generated by the longer azide linker on the alginate-hN_3. The type of alginate used to form the inner capsule also resulted in modulation of permselectivity (Figure 3C). Coatings assembled onto standard alginate microcapsules resulted in a significantly higher permselectivity, i.e. MWCO of $70{\times}10^3$ for alginate, compared to the $500{\times}10^3$ g/mol found for coatings on alginate-N_3 base materials (see Table 3). This result was initially unexpected, given the prediction that PAMAM/alginate-hN_3 coatings would be more stable on alginate-N_3 microbeads, given the increased opportunity for covalent bond linkage to the base microbead. Since the inner hydrogel core is chelated and hence a liquid prior to measurement of permeability, these results cannot be attributed to variation in the permselectivity of the inner alginate hydrogel.

Surface imaging of coatings on alginate microbeads versus microcapsules

We postulated that the increase in permselectivity for alginate capsules coated with layers that used PAMAM 15/40 or PLL, when compared to alginate-N_3 capsules coated with the same polymers, could be due to the increased swelling of the inner alginate microbead following chelation. As summarized in Table 2, when alginate hydrogel was used as the microbead material, liquification of the hydrogel following coating with PAMAM/alginate-hN_3 layers resulted in ~2.5 fold increase in swelling, when compared to the same coatings formed on alginate-N_3 beads. As such, following the formation of the ultrathin coating, the substantial swelling of the inner alginate core can result in alterations of the coating features. This hypothesis was explored via surface imaging of the coatings pre- and post-chelation using atomic force microscopy (AFM) imaging. As demonstrated in Figure 4, the topography of the coatings generated using PAMAM 15/0, PAMAM 15/20, or PAMAM 15/40 were markedly different. Further, the conversion of the alginate hydrogel to a liquefied core resulted in changes in topography for all coatings, in particular those that employed PAMAM 15/40. Analysis of the images found the root-mean-square (RMS) deviation of the surface, which provides a measurement of the surface roughness, to be the highest in the PAMAM 15/20 (58.8+3.8 nm) and PAMAM 15/40 (57.8±10.5 nm) coatings and lowest in the PAMAM 15/0 (35.5±6.9 nm), pre-chelation. Surface roughness in all coatings was significantly reduced after EDTA chelation process, with coatings formed using PAMAM 15/40 exhibiting the most significant decrease in RMS. This modification in the coating structure provides some insight as to the effect of capsule swelling on coating structure. A decrease in RMS was also observed for PLL coated capsules (see

Supplementary Materials). These results do not provide definitive correlations between coating structure and permselectivity, but provides the basis for the focus of future studies.

Cytotoxicity and insulin secretion from PAMAM/alginate coatings

Alginate capsules are commonly used for the microencapsulation of cells for the release of therapeutic agents. With the potential of these coatings to provide a versatile platform for generating stable microcapsules of modulated permselectivity, we sought to evaluate the cytotoxicity of these coatings. Further, with the alginate encapsulation of insulin secreting cells for treatment of diabetes of particular interest, we sought to validate the diffusion of insulin out of the coated capsules following encapsulation of beta cells. This is particularly important due to the fact that variation in permeability between idealized linear, nonionic molecules (such as dextran) and nonlinear, charged proteins (such as insulin) has been well documented. With this objective, MIN6 cells, a beta cell line, were encapsulated within standard alginate microbeads, followed by the generation of 6 layers of PAMAM/alginate-hN_3 coatings using PAMAM 15/0, PAMAM 15/20, and PAMAM 15/40. Cytotoxicity of the procedure was evaluated via live/dead confocal imaging. As illustrated in Figure 5A, no substantial variation in beta cell viability was observed for PAMAM/alginate-hN_3 coated capsules, particularly when compared to alginate/PLL capsules, although it could be interpreted that PAMAM 15/0 coated beads exhibited a slightly higher degree of peripheral cell death. High cytocompatibility of these coatings was expected, given our published report on the general cytocompatibility of these PAMAM/alginate-hN_3 layers when coated directly onto a pancreatic islet[40]; however, for coatings formed using PAMAM 15/0, a modest decrease in pancreatic islet viability was noted, which may correlate to the trend observed herein. The ability of insulin, released by the entrapped beta cells, to permeate out of the coated capsules was also assessed and compared to PLL/Alg controls (Figure 5B). Insulin release was significantly lower for PAMAM 15/0 coatings, when compared to PLL coated capsules, while other tested coatings were comparable. This decrease could be due to a decreased number of viable cells within the capsule or an increased restriction in insulin diffusion from the coating. Decreased cell viability cannot be ruled out, since a modest increase in dead cells could be interpreted in the live/dead imaging. With respect to insulin diffusion from the coating, permeability testing for alginate coated microcapsules found a significant decrease in coating permeability between 4×10^3 and 10×10^3 g/mol dextrans for coatings assembled using PAMAM 15/0, indicating that decreased diffusion of agents within that molecular weight range, such as insulin (MW 5.8×10^3 g/mol), may be observed. Further, the charge of PAMAM 15/0 is highly cationic (+110), which may contribute to delayed diffusion of the slightly anioic insulin. Overall, these results demonstrate the capacity of insulin to be released from these coatings; although coatings generated using PAMAM 15/0 may impart a delay in insulin migration out of the capsule and thus might not be as suitable as other PAMAM derivatives for this particular application.

Biocompatibility of PAMAM/alginate coating

The biocompatibility of the PAMAM/alginate is a critical parameter in establishing the relevance of these coatings for *in vivo* translation. To explore their compatibility, alginate microbeads coated with PAMAM/alginate-hN_3 layers generated using PAMAM 15/0 were used. With the well documented challenges of cations with biocompatibility,[28, 52, 53] we

selected coatings formed using PAMAM 15/0, as this was most likely candidate to instigate an undesirable foreign body response. Alginate microbeads were coated with either 6 layers of PAMAM/alginate or 7 layers of PAMAM/alginate, to evaluate of the impact of the surface polymer, i.e. PAMAM 15/0 or hyperbranched alginate-N_3, on the host response. Uncoated alginate microbeads were used as controls. As exhibited in Figure 6, a significant foreign body response to the capsules was not observed after 21 d *in vivo*. In general, the host response to all capsules was modest, with no deposition of cells on most capsules and only a few atypical microbeads with 1–3 layer thick cellular coatings. In general, a foreign body response is most aggressive within the first 30 days of transplant.[54, 55] As such, this study exhibits high biocompatibility of PAMAM/alginate coated capsules, with minimal foreign body responses when transplanted within the peritoneal site. Future studies will expand assessments to additional formations and transplant sites, with and without encapsulated cells.

CONCLUSIONS

Alginate beads were successfully coated in a layer-by-layer manner upon alternating functionalized PAMAMs with hyperbranched alginate azide. Coatings were found to be stable, preserving bead integrity following liquification of the inner alginate core. Modulation of permselectivity of the resulting capsules was achieved via manipulation of charge, layer number, and length of the functionalized arms, providing a highly tailorable approach. Resulting beads performed well as cell carriers and demonstrated high compatibility *in vivo*. Overall, deposition of PAMAM/alginate-hN_3 nanoscale coatings provides a unique alternative to standard polycations coatings for imparting stability and permselectivity of alginate microbeads.

Supplementary Material

Refer to Web version on PubMed Central for supplementary material.

Acknowledgments

This work was supported by the National Institutes of Health through the Type 1 Diabetes Pathfinder Award Program (1DP2 DK08309601) and NIDDK (R01 DK100654), as well as the Diabetes Research Institute Foundation. We thank the DRI Analytical Imaging Core for use of their facilities. We thank Courtney Brutman, NIH NIDDK Step-UP summer intern, for his technical assistance with this project. Finally, we thank Dr. Camillo Ricordi, Director of the Diabetes Research Institute, for his continual guidance, support, and consult.

REFERENCES

1. Kim B, Bowersock T, Griebel P, Kidane A, Babiuk LA, Sanchez M, Attah-Poku S, Kaushik RS, Mutwiri GK. J. Controlled Release. 2002; 85:191–202.
2. Bowersock TL, Hogenesch H, Suckow M, Guimond P, Martin S, Borie D, Torregrosa S, Park H, Park K. Vaccine. 1999; 17:1804–1811. [PubMed: 10194843]
3. Gombotz WR, Wee SF. Adv. Drug Del. Rev. 2012; 64(Supplement):194–205.
4. Shoichet MS, Winn SR. Adv Drug Deliv Rev. 2000; 42:81–102. [PubMed: 10942816]
5. Hasse C, Bohrer T, Barth P, Stinner B, Cohen R, Cramer H, Zimmermann U, Rothmund M. World J. Surg. 2000; 24:1361–1366. [PubMed: 11038207]
6. Giraldo JA, Weaver JD, Stabler CL. Journal of Diabetes Science & Technology. 2010; 4:1238–1247. [PubMed: 20920446]

7. Read T-A, Sorensen DR, Mahesparan R, Enger PO, Timpl R, Olsen BR, Hjelstuen MHB, Haraldseth O, Bjerkvig R. Nat Biotech. 2001; 19:29–34.
8. Barminko J, Kim JH, Otsuka S, Gray A, Schloss R, Grumet M, Yarmush ML. Biotechnol. Bioeng. 2011; 108:2747–2758. [PubMed: 21656712]
9. Jose S, Hughbanks ML, Binder BYK, Ingavle GC, Leach JK. Acta Biomater. 2014; 10:1955–1964. [PubMed: 24468583]
10. Jacobs-Tulleneers-Thevissen D, Chintinne M, Ling Z, Gillard P, Schoonjans L, Delvaux G, Strand BL, Gorus F, Keymeulen B, Pipeleers D. Diab tologia. 2013; 56:1605–1614.
11. Elliott RB, Escobar L, Tan PL, Muzina M, Zwain S, Buchanan C. Xenotransplantation. 2007; 14:157–161. [PubMed: 17381690]
12. Calafiore R, Basta G, Luca G, Lemmi A, Montanucci MP, Calabrese G, Racanicchi L, Mancuso F, Brunetti P. Diabetes Care. 2006; 29:137–138. [PubMed: 16373911]
13. Tuch BE, Keogh GW, Williams LJ, Wu W, Foster JL, Vaithilingam V, Philips R. Diabetes Care. 2009; 32:1887–1889. [PubMed: 19549731]
14. de Vos P, Hamel AF, Tatarkiewicz K. Diab tologia. 2002; 45:159–173.
15. O'Sullivan ES, Vegas A, Anderson DG, Weir GC. Endocr. Rev. 2011; 32:827–844. [PubMed: 21951347]
16. de Vos P, Bucko M, Gemeiner P, Navratil M, Svitel J, Faas M, Strand BL, Skjak-Braek G, Morch YA, Vikartovska A, Lacik I, Kollarikova G, Orive G, Poncelet D, Pedraz JL, Ansorge-Schumacher MB. Biomaterials. 2009; 30:2559–2570. [PubMed: 19201460]
17. Stabler C, Wilks K, Sambanis A, Constantinidis I. Biomaterials. 2001; 22:1301–1310. [PubMed: 11336302]
18. McDowell, RH. Properties of Alginates. 4th edn.. London: Alginate Industries Ltd; 1977.
19. Haug A, Larsen B, Smidsrød O. Carbohydr. Res. 1974; 32:217–225.
20. Thu B, Bruheim P, Espevik T, Smidsrod O, Soon-Shiong P, Skjak-Braek G. Biomaterials. 1996; 17:1069–1079. [PubMed: 8718966]
21. Benson JP, Papas KK, Constantinidis I, Sambanis A. Cell Transplant. 1997; 6:395–402. [PubMed: 9258513]
22. de Vos P, Lazarjani HA, Poncelet D, Faas MM. Adv. Drug Del. Rev. 2014; 67–68:15–34.
23. De Castro M, Orive G, Hernandez RM, Gascon AR, Pedraz JL. J. Microencapsul. 2005; 22:303–315. [PubMed: 16019916]
24. Bunger CM, Gerlach C, Freier T, Schmitz KP, Pilz M, Werner C, Jonas L, Schareck W, Hopt UT, de Vos P. Journal of biomedical materials research. Part A. 2003; 67:1219–1227. [PubMed: 14624508]
25. de Vos P, van Hoogmoed CG, van Zanten J, Netter S, Strubbe JH, Busscher HJ. Biomaterials. 2003; 24:305–312. [PubMed: 12419632]
26. Ponce S, Orive G, Hernández R, Gascón AR, Pedraz JL, de Haan BJ, Faas MM, Mathieu HJ, de Vos P. Biomaterials. 2006; 27:4831–4839. [PubMed: 16766026]
27. Hunter AC. Adv. Drug Del. Rev. 2006; 58:1523–1531.
28. Chanana M, Gliozzi A, Diaspro A, Chodnevskaja I, Huewel S, Moskalenko V, Ulrichs K, Galla H-J, Krol S. Nano Lett. 2005; 5:2605–2612. [PubMed: 16351223]
29. Hong S, Leroueil PR, Janus EK, Peters JL, Kober M-M, Islam MT, Orr BG, Baker JR, Banaszak Holl MM. Bioconjug. Chem. 2006; 17:728–734. [PubMed: 16704211]
30. Fischer D, Li Y, Ahlemeyer B, Krieglstein J, Kissel T. Biomaterials. 2003; 24:1121–1131. [PubMed: 12527253]
31. Zhang X, Chen H, Zhang H. Chem. Commun. 2007:1395–1405.
32. Tong W, Song X, Gao C. Chem. Soc. Rev. 2012; 41:6103–6124. [PubMed: 22695830]
33. Huang C-J, Chang F-C. Macromolecules. 2009; 42:5155–5166.
34. Buck ME, Lynn DM. Langmuir. 2010; 26:16134–16140. [PubMed: 20857952]
35. Lvov Y, Decher G, Moehwald H. Langmuir. 1993; 9:481–486.
36. Decher G, Hong J-D. Makromolekulare Chemie. Macromolecular Symposia. 1991; 46:321–327.
37. Sato K, Anzai J-i. Molecules. 2013; 18:8440–8460. [PubMed: 23867653]

38. Paez JI, Brunetti V, Strumia MC, Becherer T, Solomun T, Miguel J, Hermanns CF, Calderon M, Haag R. J. Mater. Chem. 2012; 22:19488–19497.
39. Best MD. Biochemistry (Mosc). 2009; 48:6571–6584.
40. Gattás-Asfura KM, Stabler CL. ACS Applied Materials & Interfaces. 2013; 5:9964–9974. [PubMed: 24063764]
41. Gattas-Asfura KM, Fraker CA, Stabler CL. Journal of biomedical materials research. Part A. 2011; 99:47–57. [PubMed: 21793196]
42. Gattas-Asfura KM, Stabler CL. Biomacromolecules. 2009; 10:3122–3129. [PubMed: 19848408]
43. Sun AM. Methods Enzymol. 1988; 137:575–580. [PubMed: 3131633]
44. Lilla V, Webb G, Rickenbach K, Maturana A, Steiner DF, Halban PA, Irminger J-C. Endocrinology. 2003; 144:1368–1379. [PubMed: 12639920]
45. Briššová M, Petro M, Lacík I, Powers AC, Wang T. Anal. Biochem. 1996; 242:104–111. [PubMed: 8923972]
46. King A, Sandler S, Andersson A. J. Biomed. Mater. Res. 2001; 57:374–383. [PubMed: 11523032]
47. Wang Y-C, Tang L-Y, Li Y, Wang J. Biomacromolecules. 2008; 10:66–73. [PubMed: 19133835]
48. Tam SK, Dusseault J, Bilodeau S, Langlois G, Hallé J-P, Yahia LH. Journal of Biomedical Materials Research Part A. 2011; 98A:40–52. [PubMed: 21523903]
49. Darrabie MD, Kendall WF Jr, Opara EC. Biomaterials. 2005; 26:6846–6852. [PubMed: 15955558]
50. Thu B, Bruheim P, Espevik T, Smidsrød O, Soon-Shiong P, Skjåk-Bræk G. Biomaterials. 1996; 17:1031–1040. [PubMed: 8736740]
51. Draget KI, Skjåk-Bræk G, Smidsrød O. Int. J. Biol. Macromol. 1997; 21:47–55. [PubMed: 9283015]
52. Strand BL, Ryan TL, In't Veld P, Kulseng B, Rokstad AM, Skjak-Brek G, Espevik T. Cell Transplant. 2001; 10:263–275. [PubMed: 11437072]
53. Juste S, Lessard M, Henley N, Menard M, Halle JP. Journal of biomedical materials research. Part A. 2005; 72:389–398. [PubMed: 15669081]
54. Orive G, Tam SK, Pedraz JL, Hallé J-P. Biomaterials. 2006; 27:3691–3700. [PubMed: 16574222]
55. Onuki Y, Bhardwaj U, Papadimitrakopoulos F, Burgess DJ. J Diabetes Sci Technol. 2008; 2:1003–1015. [PubMed: 19885290]

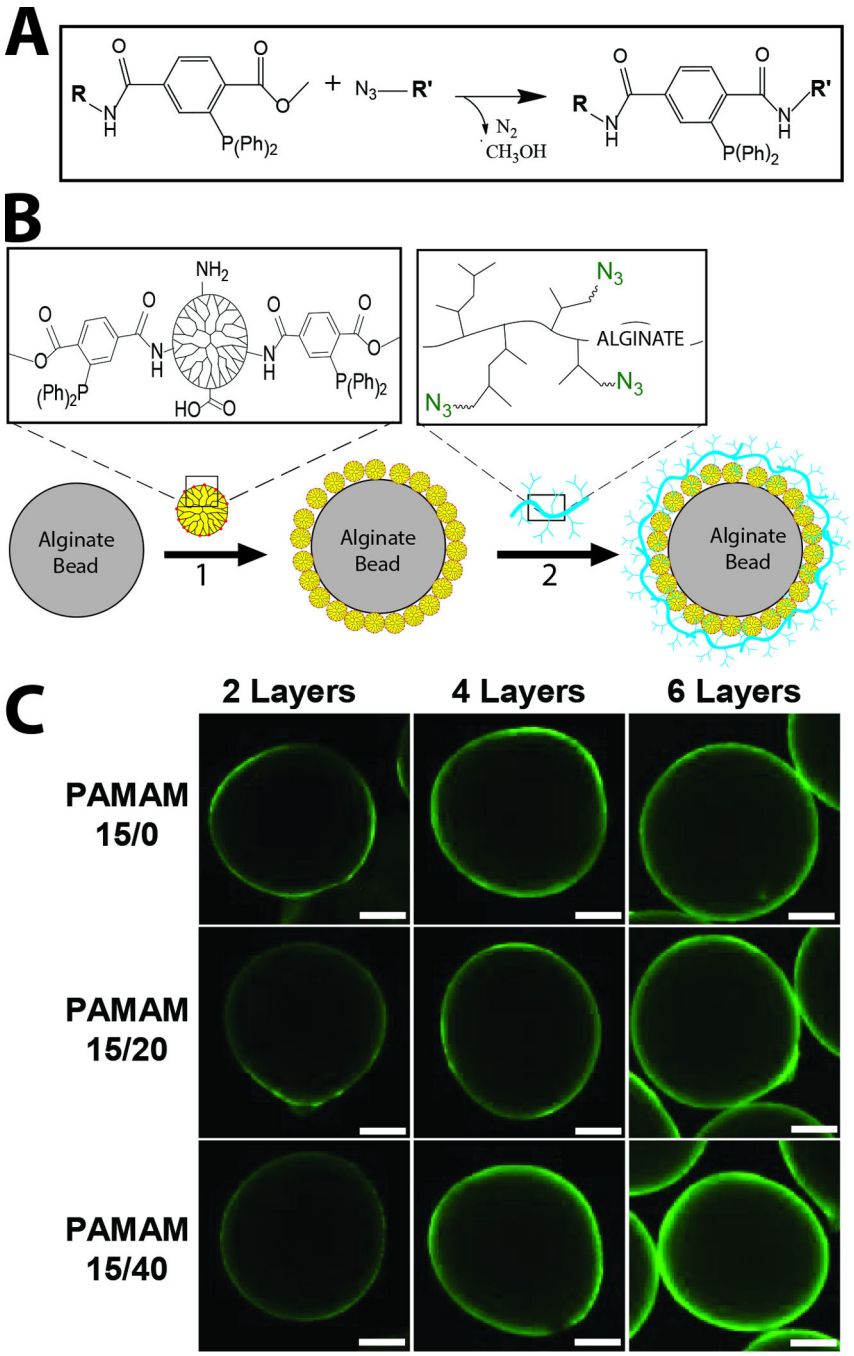

Figure 1.

A) Schematic of Staudinger Ligation reaction when within aqueous solution. **B)** Schematic of ultrathin coating assembly onto alginate microbeads. Alginate microbeads were first incubated in MDT functionalized PAMAM (1). Subsequently, hyperbranched alginate azide was covalently linked to the exposed MDT functionalized PAMAM coating (2). Interlayer covalent bonds were formed between complementary azide and MDT groups via Staudinger ligation. Additional layers were built via step-wise incubation of MDT functionalized PAMAM (1) and hyperbranched alginate azide (2), until desired number of layers were

achieved. **C)** Visualization of coating generated on alginate microbeads via step-wise layer formation using hyperbranched alginate azide (labeled with FITC for confocal imaging) and PAMAM 15/0, PAMAM 15/20, or PAMAM 15/40. Images were collected after 2, 4, and 6 layers were applied. Scale = 200 μm.

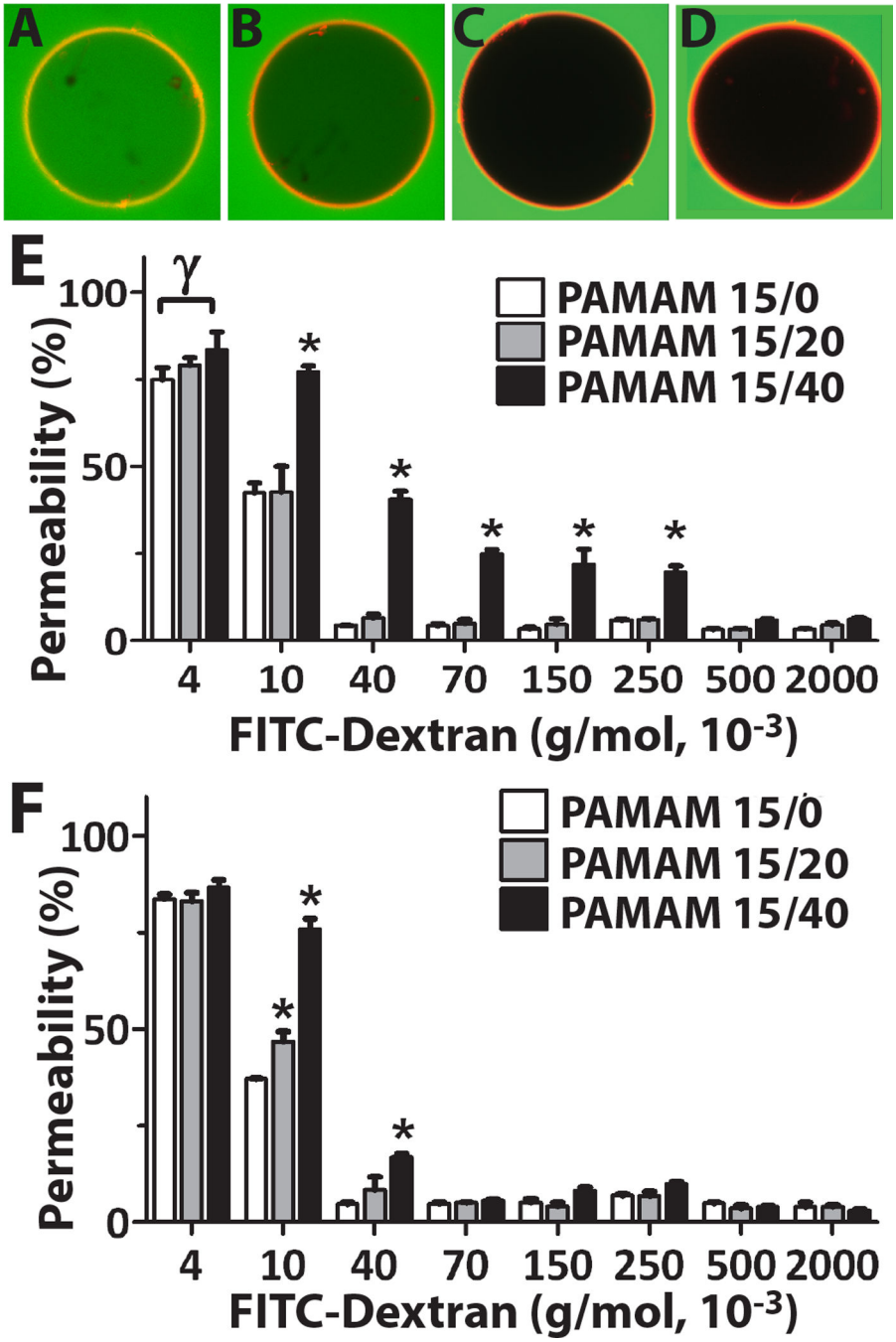

Figure 2.

Comparison of permselectivity for coatings on alginate-N_3 versus standard alginate microcapsules. Representative confocal images of coated capsules (alginate-N_3 coated with 6 layers of PAMAM 15/0 and alginate-hN_3) collected 2 h after incubation with **(A)** 4, **(B)** 10, **(C)** 40, or **(D)** 70 $\times 10^3$ g/mol FITC-Dextran. Quantification of % permeability of FITC-Dextran label for alginate-N_3 **(E)** and alginate **(F)** microcapsules coated with 6 layers of PAMAM/alginate-hN_3, where PAMAM 15/0 (white bars), PAMAM 15/20 (grey bars), or

PAMAM 15/40 (black bars) were employed. *Statistically different from all other coatings ($P < 0.05$); Statistically different from selected coating ($P < 0.05$)

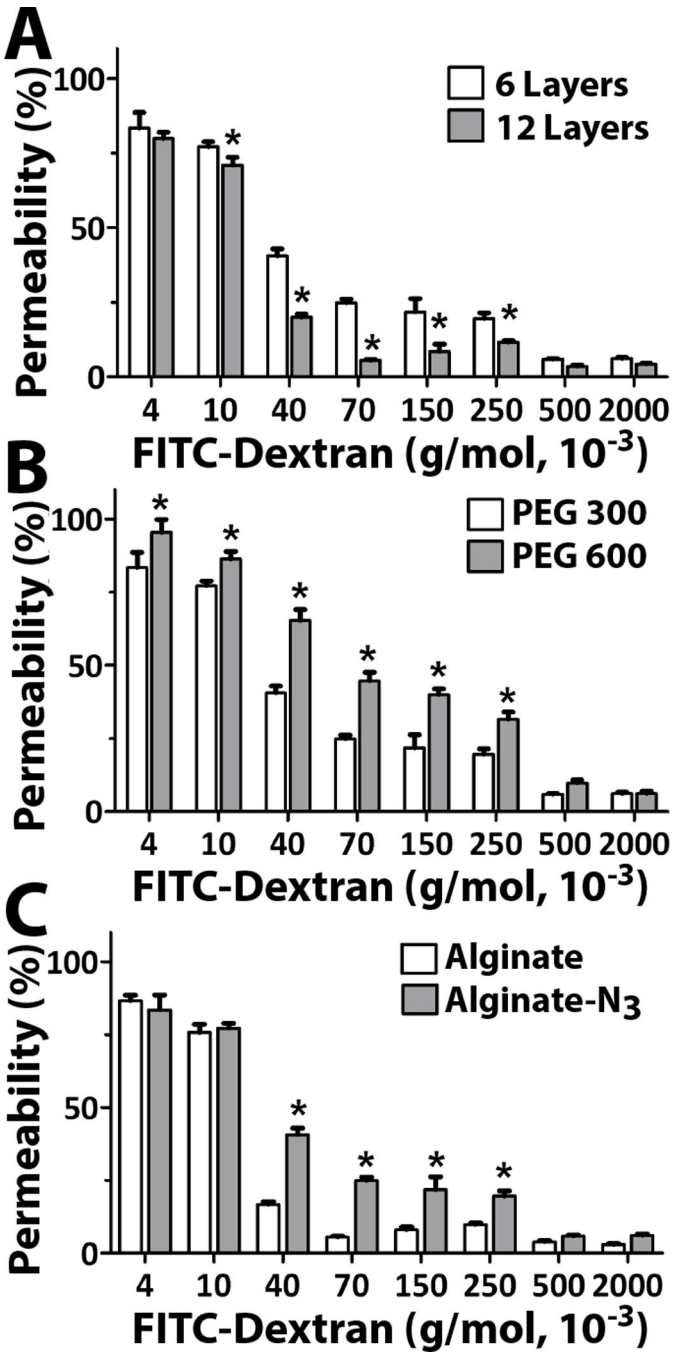

Figure 3.

Evaluation of coating parameters on permselectivity for capsules were coated with PAMAM 15/40 and hyperbranched alginate-hN_3. The effect of the: A) number of layers; B) length of PEG-N_3 linker used to functionalize the hyperbranched alginate-azide; and C) alginate capsule, alginate or alginate-N_3, was evaluated. *Statistically different from other groups ($P < 0.05$)

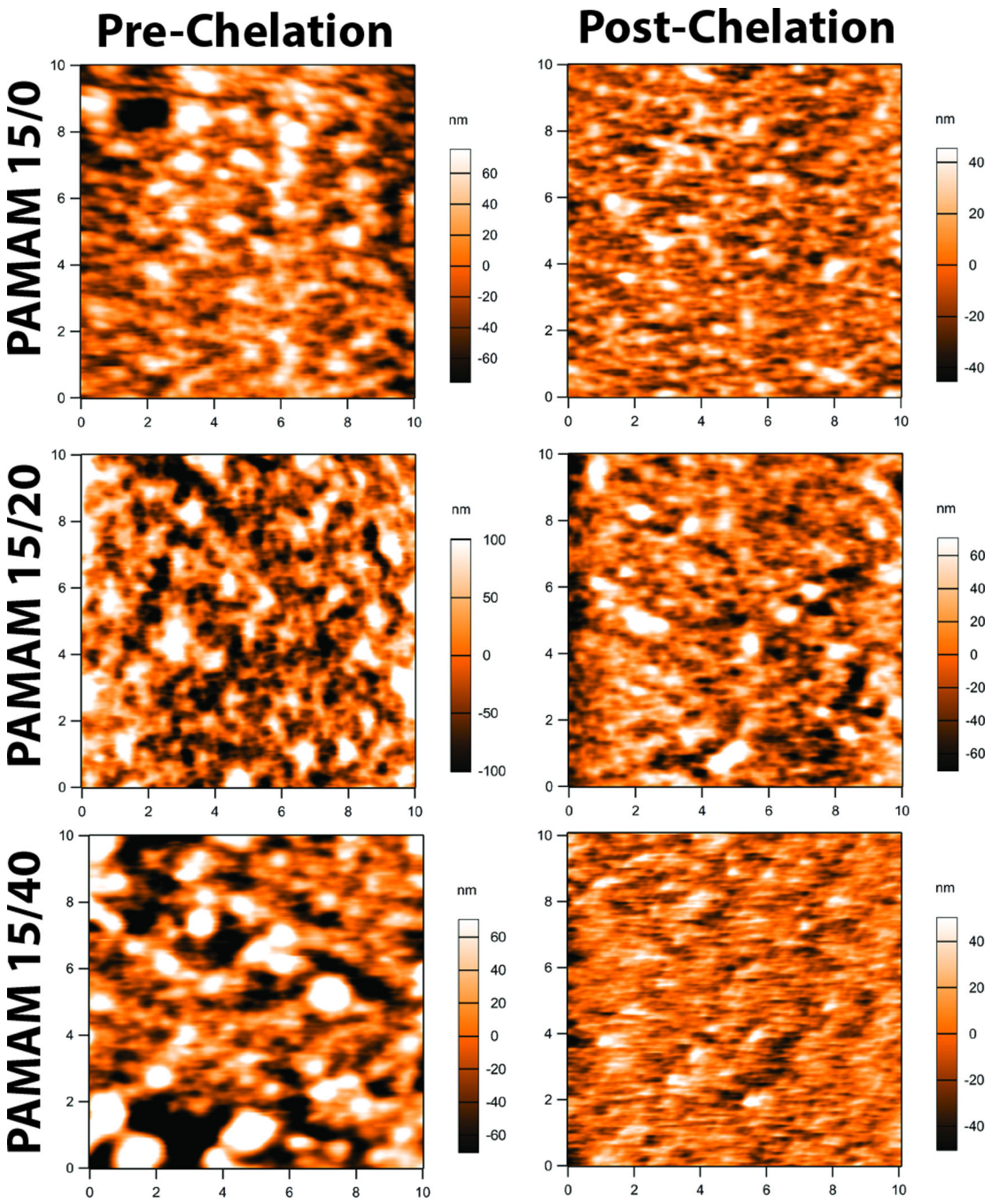

Figure 4.

Atomic force microscopy images of alginate coated with 6 layers of PAMAM/alginate-hN_3 using PAMAM 15/0 (top row), PAMAM 15/20 (middle row), and PAMAM 15/40 (bottom row). Images were collected pre (left) and post (right) exposure to EDTA to chelate the inner alginate microbead. Image size was 10 × 10 μm. Scale shown to right of each figure, in nm.

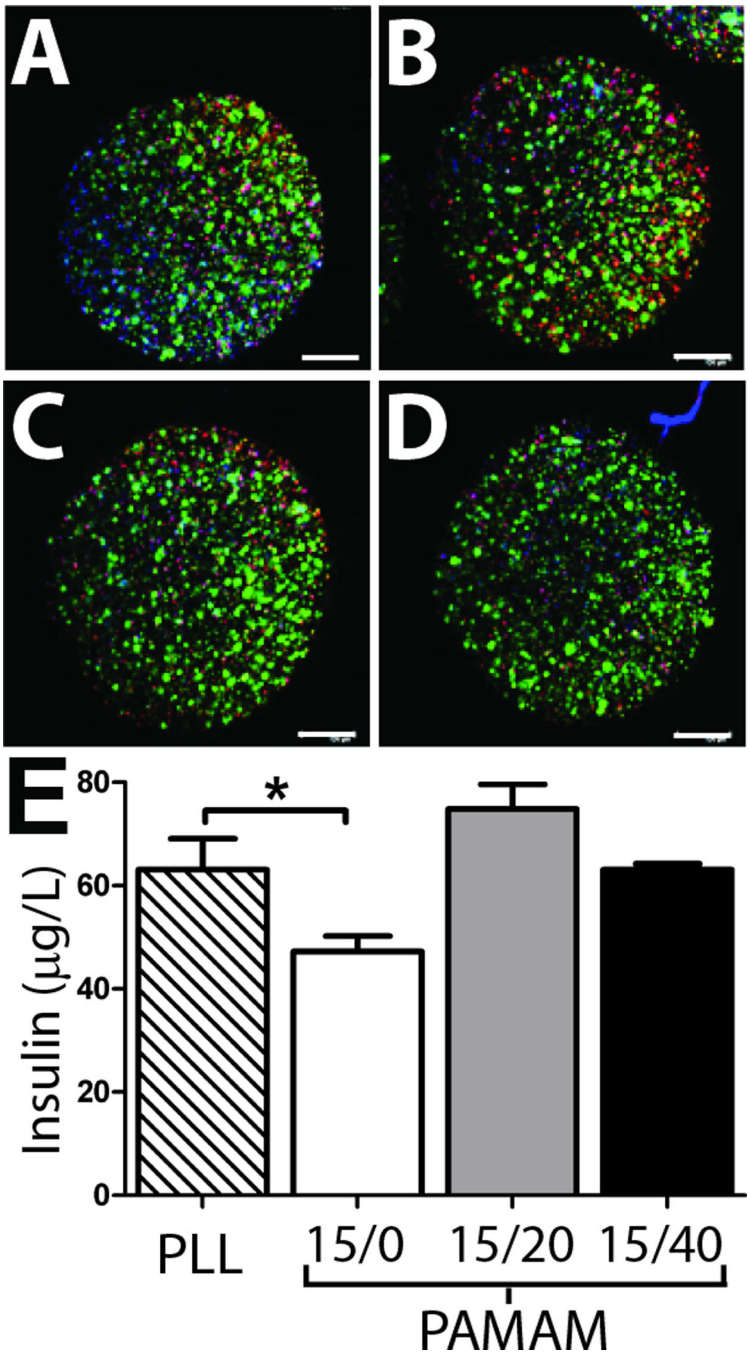

Figure 5.

Evaluation of cytocompatibility and insulin release from alginate capsules. Confocal images of beta cells encapsulated within alginate capsules coated with PLL (A) or 6 layers of PAMAM/alginate using PAMAM 15/0 (B), PAMAM 15/20 (C), or PAMAM 15/40 (D). Live (green); dead (red); nuclei (blue). Scale = 200 µm. E) Insulin release from entrapped beta cells encapsulated within alginate capsules coated with PLL (striped bar) or 6 layers of PAMAM/alginate using PAMAM 15/0 (white bar), PAMAM 15/20 (grey bar), or PAMAM

15/40 (black bar). All values are statistically different from each other ($P < 0.05$), except PLL and PAMAM 15/40. * $p < 0.05$

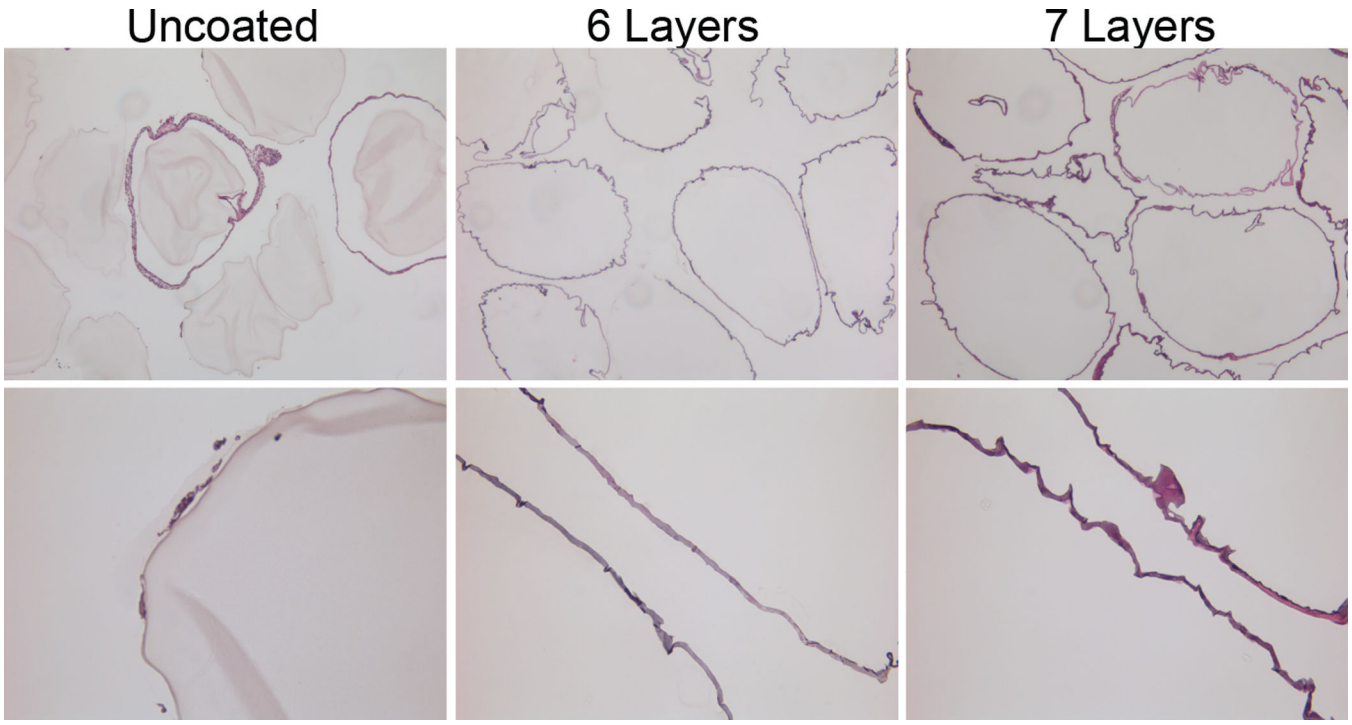

Figure 6.

H/E staining of alginate microbeads, explanted from mice 21 d post transplantation. Uncoated alginate microbeads (left panel) were compared to alginate microbeads coated with 6 (middle panel) or 7 (right panel) layers of PAMAM/alginate, formed using PAMAM 15/0. Layers with 6 coatings had a final layer of hyperbranched alginate-azide, while 7 layer coatings had a final layer of PAMAM 15/0. Note: Hematoxylin binds to the PAMAM dendrimer, resulting in staining of outer coating. Magnification: top row: 5×; bottom row: 20×

Table 1

Properties of selected PAMAM derivatives with varying MDT and GA functionalization. Charge and molecular weight were calculated as described in previous publication[40].

PAMAM (ID)	MDT (%)	GA (%)	Net Charge	MW (g/mol)
15/0	14	0	+110	35,026
15/20	14	23	+ 51	38,412
15/40	14	44	−3	41,503

Table 2

% swelling of coated alginate-N_3 or alginate capsules following removal of barium via EDTA. Layers of PAMAM/Alginate (6 or 12 in total) were generated using PAMAM 15/0, PAMAM 15/20, and PAMAM 15/40 and hyperbranched alginate-azide. The standard PEG-azide linker (300 MW) was used for all coatings except PAMAM 15/40†, which used the longer PEG-azide linker (600 MW). NC = experiment not conducted.

	Alginate-Azide		Alginate
PAMAM	**6 layers**	**12 layers**	**6 layers**
15/0	17.3±1.8	NC	43.8±2.9
15/20	14.4±1.7	3.4±0.9	29.9±2.9
15/40	14.4±1.4	5.9±2.0	37.0±3.1
15/40†	31.7±3.2	8.8±1.3	NC
PLL/Alg	−1.6±0.4		39.4±3.1

Table 3

Permselectivity of alginate-N_3 or alginate capsules coated with 6 layers of PAMAM/Alginate-hN_3 using PAMAM 15/0, PAMAM 15/20, and PAMAM 15/40 and alginate-hN_3. Results were compared to PLL/Alg control coating. R_h= theoretical hydrodynamic radius

	Microcapsule Base Material	
PAMAM	**Alginate-Azide**	**Alginate**
15/0	MW = 40×10^3 g/mol R_h = 4.9 nm	MW = 40×10^3 g/mol R_h = 4.9 nm
15/20	MW = 40×10^3 g/mol R_h = 4.9 nm	MW = 40×10^3 g/mol R_h = 4.9 nm
15/40	MW = 500×10^3 g/mol R_h = 17.2 nm	MW = 70×10^3 g/mol R_h = 6.5 nm
PLL/Alg	MW = $2{,}000\times10^3$ g/mol Rh = 34.2 nm	MW = 70×10^3 g/mol Rh = 6.5 nm